Cygnus A

A. S. Wilson, K. A. Arnaud[1], D. A. Smith, Y. Terashima[2], A. J. Young

Astronomy Department, University of Maryland, College Park, MD 20742, U.S.A.

ABSTRACT

We report Chandra imaging-spectroscopy and RXTE spectroscopy of the nearby, powerful radio galaxy Cygnus A. Various aspects of the results are discussed, including the X-ray properties of the nucleus, the radio hot spots, the cluster of galaxies, the prolate cavity in the ICM inflated by the radio jets and "bands" of thermal gas which encircle the cavity in its equatorial plane. The hard X-ray emission of the nucleus extends to 100 keV and originates from an unresolved source absorbed by a large column density ($N_H \simeq 2 \times 10^{23}$ cm^{-2}) of gas. The soft (< 2 keV) nuclear emission exhibits a bipolar structure which extends $\simeq 2$ kpc from the nucleus and is strongly correlated with both optical continuum and emission-line morphologies. It is suggested that this nebulosity is photoionized by the nucleus and that the extended X-rays are electron-scattered nuclear radiation. All four radio hot spots are detected in X-rays, with the emission resulting from synchrotron self-Compton radiation in an approximately equipartition field. The temperature of the X-ray emitting intracluster gas drops from $\simeq 8$ keV more than 100 kpc from the center to $\simeq 5$ keV some 80 kpc from the center, with the coolest gas immediately adjacent to the radio galaxy. There is a metallicity gradient in the X-ray emitting gas, with the highest metallicities ($\sim$ solar) found close to the center, decreasing to ~ 0.3 solar in the outer parts. We have used the assumption of hydrostatic equilibrium to derive a total cluster mass within 500 kpc of 2.0×10^{14} $M_\odot$ and 2.8×10^{14} $M_\odot$, and a gas fraction in the cluster within 500 kpc of 0.055 and 0.039 for a constant and centrally decreasing temperature profile, respectively. We show that the limb-brightened edge of the cavity is hotter than the nearby, innermost region of the cluster gas, indicating heating by the expanding, jet-driven cavity. Conversely, the "bands", interpreted as gas being accreted onto the galaxy, are cooler. Within the cavity, there is evidence for diffuse X-ray emission, in addition to the X-ray emissions related to the jets and hot spots.

Subject headings: galaxies: active – galaxies: clusters – galaxies: individual (Cygnus A) – galaxies: nuclei – galaxies: X-rays – intergalactic medium – interstellar medium

---

[1]Laboratory for High Energy Astrophysics, NASA/GSFC, Code 662, Greenbelt, MD 20771, U.S.A.

[2]Institute of Space and Aeronautical Science, 3-1-1 Yoshinodai, Sagamihara, Kanagawa 229-8510, Japan

1. Introduction

Cygnus A is a powerful radio galaxy that is unusually close to us (z = 0.0562, Stockton et al. 1994). Its radio luminosity is more than two orders of magnitude above the Fanaroff-Riley I/II boundary and 1.5 orders of magnitude more luminous than any other source at z ≤ 0.1 (Carilli & Barthel 1996). Most sources with similar radio luminosities are found at z = 1 and beyond. For these reasons, Cyg A is considered the archetypal powerful radio galaxy and has been extensively studied in all wavebands.

In this paper, we summarise results from a study of Cyg A with the Chandra X-ray Observatory. Cyg A was observed with the spectroscopic array of CCDs, with the nucleus at the aim point on chip S3; the date of observation was chosen so that the extension some 15′ to the NW (Arnaud et al. 1984; Reynolds & Fabian 1996) was also imaged. An image of the 6 CCDs which were read out is shown in Fig. 1. The Cyg A cluster is the bright region near the center and the putative other cluster is seen to the NW.

An enlargement of the inner region, on the scale of the double radio source, is given in Fig. 2 and shows a wealth of structure. The brightest region, in the center, is the galaxy nucleus. The "hot spots" (two bright ones about 1′ to the NW and one bright and one faint one a similar distance to the SE) coincide with the radio hot spots. There are two diffuse, linear structures running from the nucleus towards each pair of hot spots; these quasi-linear features seem to be associated with the radio jets, though in X-rays the emission is more diffuse. The overall, prolate shape presumably represents the limb-brightened cavity inflated in the intracluster medium (ICM) by relativistic particles that have escaped from the hot spots, as predicted by Scheuer (1974). The whole structure is embedded in the ICM of the cluster of galaxies, which extends to a much larger scale (see Fig. 1). Lastly, curved "bands" run transversely (i.e. NE - SW) across the cavity and appear to be the projections of rings of gas which encircle it; if the plane of these rings is perpendicular to the radio axis, the rings must be predominantly on the far side of the cavity since the jet to the NW is the nearer. We discuss these various features in turn and refer the reader to Wilson et al. (2000, Paper I, about the "hot spots"), Young et al. (2002, Paper II, about the nucleus) and Smith et al. (2002, Paper III, about the cluster) for further details.

2. The nucleus

Fig. 3 shows a color representation of the Chandra X-ray image of the nuclear region. The data were divided into 3 bands, red representing 0.1 - 1.275 keV, green 1.275 - 2.2 keV and blue 2.2 - 10 keV. There is a hard X-ray, unresolved, core source, and extended bi-polar soft nebulosity, the latter correlating well with the optical bi-polar continuum and emission-line structures (e.g. Fig. 4) and being approximately aligned with the radio jet. The bi-polar X-ray morphology may be enhanced by absorption by the dust lane crossing the nucleus, suppressing the very soft X-ray emission.

We obtained quasi-simultaneous Chandra - RXTE observations in order to define the broad-band spectrum. The main spectral results are: 1) the compact nucleus is detected to 100 keV and is well described by a heavily absorbed power law spectrum with $\Gamma_h = 1.52 \pm 0.12$ and equivalent hydrogen column N_H (nuc) = $2.0^{+0.1}_{-0.2} \times 10^{23}$ cm^{-2}. This column is compatible with the dust obscuration to the near infrared source for a normal gas to dust ratio; 2) the soft (< 2 keV) emission from the nuclear region may be described by a power law spectrum with a similar index ($\Gamma_l \simeq \Gamma_h$). Narrow emission lines from highly ionized neon and silicon are observed in the soft X-ray spectrum of the NW and SE regions; 3) A "neutral" Fe Kα line is detected in the nucleus and its vicinity (r $<$ 2 kpc). The equivalent width (EW) of this line is in good agreement with theoretical predictions for the EW versus N_H(nuc) relationship in various geometries. An Fe K edge is also seen (Fig. 5). Comparing this edge with N_H(nuc), the nuclear iron abundance is found to be essentially solar.

Extrapolation of the best power law model of the soft (0.5 – 2 keV), extended, circumnuclear emission to higher energies gives a 2 – 10 keV luminosity of $\simeq 3.7 \times 10^{42}$ erg s^{-1}, which is 1% of that of the unabsorbed nuclear luminosity in the same band. As noted above, the photon index (Γ_l) of this soft emission agrees with that (Γ_h) of the directly viewed hard X-ray emission, and so the soft emission is consistent with being electron-scattered X-rays from the nucleus. The scattering region must be ionized to ionization parameter $\xi \geq 1$ in order to be sufficiently transparent to soft X-rays. The column density of the scattering electrons is inferred to be much lower than that required to generate the extended polarized optical light by electron scattering, suggesting the optical light is, in fact, scattered by dust. The excellent spatial correlation between the extended soft X-ray emission and the ionized gas observed optically with HST (Fig. 4) is consistent with the soft X-ray emitting gas being photoionized.

3.   The hot spots

Radio hot spots A, B, D and E are detected in the Chandra image (note that the originally defined 'C' is no longer considered a hot spot). Their location and morphology are essentially identical to those of the corresponding radio hot spots (e.g. Fig. 6). X-ray spectra have been obtained for the two brighter hot spots (A and D). Both are well described by a power law with photon index $\Gamma = 1.8 \pm 0.2$ absorbed by the Galactic column in the direction of Cygnus A. Thermal X-ray models require too high gas densities and may be ruled out. The images and spectra (e.g. Fig. 7) strongly support synchrotron self-Compton models of the X-ray emission, as proposed by Harris, Carilli & Perley (1994) on the basis of ROSAT imaging observations. Such models indicate that the magnetic field in each of the brighter hot spots is 1.5×10^{-4} gauss, with an uncertainty of a few tens of percent. This value is close to the equipartition field strengths assuming no protons are present.

It is notable that the magnetic field cannot be less than 1.5×10^{-4} gauss since the SSC radiation would then exceed the observed X-radiation. The alternative is that B $> 1.5 \times 10^{-4}$

gauss in which case the predicted SSC emission would be too weak to account for the observed X-ray emission. The X-rays would then have to be synchrotron radiation. However, we feel that the synchrotron self-Compton model is by far the more likely. Synchrotron self-Compton emission from hot spots in radio galaxies with magnetic fields close to equipartition has now been detected in 3C 123 (Hardcastle, Birkinshaw & Worrall 2001), 3C 295 (Harris et al. 2000) and Cygnus A. Thus the accumulating evidence is that equipartition between cosmic rays and magnetic fields is common in radio hot spots.

4.   The cluster of galaxies

As discussed above, the dominant gaseous structure is a roughly "football shaped" (American useage) feature with semi-major axis $\simeq 1.'1$ ($\simeq 100$ kpc), which is presumably prolate spheroidal in three dimensions. This structure apparently represents intracluster gas which has been swept up and compressed by a cavity inflated in this gas by relativistic material which has passed through the ends of the radio jets. The X-ray emitting gas shows this prolate spheroidal morphology to $\simeq 1.'2$ (110 kpc) from the radio galaxy, but is spherical on larger scales. The X-ray emission from the intracluster gas extends to at least $8'$ ($\simeq 720$ kpc) from the radio galaxy, and a second, extended source of X-ray emission (probably associated with a second cluster of galaxies) is seen some $12'$ ($\simeq 1$ Mpc) to the NW of Cygnus A. The X-ray spectrum of the integrated intracluster gas imaged on the S3 chip (dimensions $8' \times 8' = 720 \times 720$ kpc), excluding the contribution from the radio galaxy and other compact sources of X-ray emission, indicates a gas temperature, metallicity, and unabsorbed 2–10 keV rest-frame luminosity of 7.7 keV, 0.34 times solar, and 3.5×10^{44} erg s^{-1}, respectively.

The observed spectral variations in the intracluster gas are illustrated in Fig. 8, which is a color map of the softness ratio (1–2 keV/2–8 keV). The color image shows that emission inside the central $\simeq 1'$ is softer than that further out. The hardest emission is located at the position of the nucleus, which is heavily absorbed (Arnaud et al. 1987; Ueno et al. 1994; Sambruna et al. 1999; Paper II).

We have deprojected the emission from the ICM in order to measure the radial dependence of temperature, density, thermal pressure and abundance. The cluster was divided into 12 annuli, each centered on the radio galaxy. These annuli define shells in 3 dimensions. Each shell was modeled as two mekal plasmas. First, a uniform brightness mekal model (representing possible foreground Galactic emission) was added to a mekal model for the outer shell and the result was compared with the observed spectrum of the outer annulus. Both emission components were assumed to be absorbed by the same column and the model parameters for absorption and Galactic emission were subsequently fixed at their respective best-fit values. In this way, we derived the temperature, abundance, and emissivity for the outer shell of intracluster gas. Second, the spectra from the outer and adjacent shells were modeled in the same way. The temperature, abundance, and emissivity for the outer shell were fixed at the values already obtained, allowing us to derive the deprojected

temperature, abundance, and emissivity for the shell adjacent to it. This procedure was repeated for the remaining shells. In Fig. 9, we show the resulting radial dependences of gas temperature, density, metal abundance and thermal gas pressure. It is notable that the cooling time is less than the Hubble time for radii ≤ 200 kpc.

Under the assumptions of hydrostatic equilibrium and spherical symmetry, we have calculated the radial dependence of enclosed mass M($< r$) for radii 80 - 500 kpc (Fig. 10). From this analysis, we find the total mass of the cluster, within 500 kpc, is $2.0 \times 10^{14} M_\odot$ or $2.8 \times 10^{14} M_\odot$, depending on the precise temperature profile adopted (see Paper III). This compares favorably with the cluster mass of $10^{14} M_\odot$, derived from the Einstein HRI data (Arnaud et al. 1984). Within 500 kpc, the total mass of the intracluster gas is $1.1 \times 10^{13} M_\odot$.

5. The Cavity and "Belts"

Fig. 11 is an image of the region of the cavity. Regions for which spectra have been extracted are indicated by the polygons. It is very interesting that all the regions in the limb-brightened edge of the cavity are hotter than the innermost shell of the cluster (4.9±0.6 keV, see Fig. 9, top), while all regions in the transverse "belts" are cooler. While these differences in temperature are modest - up to 2.1 keV above and 1.1 keV below that of the innermost cluster shell - we believe the systematic differences between the innermost cluster shell, the limb-brightened regions and the "belts" are real. The data thus suggest that the ICM just outside the cavity is being heated by its expansion, as expected (e.g. Begelman & Cioffi 1989). In contrast, the "belts" appear to represent cooling gas in disk-like structures around, or within, the cavity. The equatorial arrangement of the disks with respect to the cavity may be interpreted in two ways:

(a) It is natural to speculate that the Cygnus A galaxy is accreting these gas disks; the gas continuously cools, falls in and ultimately fuels the accretion disk around the black hole. In this case, the radio axis of Cyg A is determined by the angular momentum of the large scale ICM.

(b) Alternatively, the radio axis might be determined in some other way, such as the spin of the black hole, either primordial or after accretion of gas or another black hole in a galaxy merger (see Stockton et al. 1994 for evidence that Cyg A has undergone a merger). When switched on, the radio jets power the radio lobes and inflate the cavity, but in view of the concentration of the lobes near the hot spots (at least at cm wavelengths), the "robustness" of the cavity in the equatorial regions may be lower than near the hot spots, allowing ICM to fall into the cavity through Kelvin-Helmholtz or Rayleigh-Taylor instabilities (which will mix the heavy ICM with the light relativistic gas given the fact that gravity points inwards). Alternatively, even if the cavity pressure is uniform (as expected if only a relativistic gas is present, so the cavity has a short sound crossing time), the expanding equatorial region may be the most unstable.

This classic "chicken and egg" problem is arguably the most important outstanding issue.

It is also of interest to determine whether there is any X-ray emitting material *inside* the cavity (in addition to the obvious "diffuse" jet-like features and the hot spots). As noted above, such emission could result, for example from ICM gas that has entered the cavity through instabilities at the cavity - ICM contact discontinuity (e.g. Reynolds, Heinz & Begelman 2002). To investigate this matter observationally, it is necessary to subtract from the image the foreground and background contributions of the cluster gas. Using our cluster model (Section 4, see also Paper III), we assume that the axis of the prolate structure is in the plane of the sky, the emission is cylindrically symmetric about this axis and that the cavity is devoid of X-ray emitting gas. The resulting model projection of a full band (0.75 - 8 keV) image of the cluster is shown in Fig. 12, top. This image may then be subtracted from the observed image, the result being shown in Fig. 12, bottom. The latter image suggests that there is, indeed, diffuse gas within the cavity. Modelled as a thermal gas, its temperature appears higher than the inner regions of the cluster (which dominate the foreground and background emission). These findings should be regarded as preliminary and the work as in progress. The main concern is that the difference map is sensitive to systematic errors in the assumed cluster model and geometry.

REFERENCES

Arnaud, K. A., Fabian, A. C., Eales, S. A., Jones, C. & Forman, W. 1984, MNRAS, 211, 981

Arnaud, K. A., Johnstone, R. M., Fabian, A. C., Crawford, C. S., Nulsen, P. E. J., Shafer, R. A., & Mushotzky, R. F. 1987,, MNRAS, 227, 241

Begelman, M. C. & Cioffi, D. F. 1989, ApJ, 345, L21

Carilli, C. L. & Barthel, P. D. 1996, Astron. Astrophys. Rev, 7, 1

Hardcastle, M. J., Birkinshaw, M. & Worrall, D. M. 2001, MNRAS, 323, L17

Harris, D. E., Carilli, C. L. & Perley, R. A. 1994, Nature, 367, 713

Harris, D. E. et al. 2000, ApJ, 530, L81

Reynolds, C. S. & Fabian, A. C. 1996, MNRAS, 278, 479

Reynolds, C. S., Heinz, S. & Begelman, M. C. 2002, MNRAS (in press) (astro-ph/0201271)

Sambruna, R. M., Eracleous, M., & Mushotzky, R. F. 1999, ApJ, 526, 60

Scheuer, P. A. G. 1974, MNRAS, 166, 513

Smith, D. A., Wilson, A. S., Arnaud, K. A., Terashima, Y. & Young, A. J. 2002, ApJ, 565, 195 (Paper III)

Stockton, A., Ridgway, S. E. & Lilly, S. J. 1994, AJ, 108, 414

Ueno, S., Koyama, K., Nishida, M., Yamauchi, S., Ward, M. J. 1994, ApJ, 431, L1

Wilson, A. S., Young, A. J. & Shopbell, P. L. 2000, ApJ (Letts), 544, L27 (Paper I)

Young, A. J., Wilson, A. S., Terashima, Y., Arnaud, K. A. & Smith, D. A. 2002, ApJ, 564, 176 (Paper II)

Fig. 1.— An image of the whole *Chandra* field in the 0.75–8 keV band. The image has been binned to a pixel size of $3.''94 \times 3.''94$. The vertical bar indicates the conversion from color to cts pixel^{-1}.

Fig. 2.— The Chandra image on the scale of the radio source. The width of the image is $2.'5$.

Fig. 3.— Color representation of the Chandra X-ray image of the nucleus of Cyg A. The data were divided into three bands, red representing 0.1 - 1.275 keV, green 1.275 - 2.2 keV and blue 2.2 - 10 keV. The nucleus coincides with a blue (hard) unresolved source and there is extended bi-polar soft emission.

Fig. 4.— A superposition of events in the range 0.25 to 1.00 keV (solid contours) on an HST image taken through a Linear Ramp Filter at redshifted [OIII] $\lambda 5007$ (grey scale).

Fig. 5.— Confidence contours (plotted at 68%, 90% and 99%) of the rest-frame energy of the iron emission line and its absorption edge. The aperture is a circle of diameter $2.''5$. The line energy is consistent with that of the Fe Kα fluorescence line of neutral iron. The absorption edge is consistent with that of iron in the range Fe I – Fe X. The panel in the upper right shows the ratio of the Chandra data to a power law as a function of rest-frame energy. To produce this panel, the data were modeled by a power law from 4 to 9 keV.

Fig. 6.— X-ray emission (contours) superposed on a 6 cm VLA radio map (grey scale) of the region of the western hot spots (A, the brighter, and B, $\simeq 6''$ SE of A). Contours are plotted at 2, 4, 8, 12, 16, 24 and 32 counts per pixel ($0.''5 \times 0.''5$). The grey scale is proportional to the square root of the radio brightness.

Fig. 7.— Spectrum of hot spot A. The points show the radio fluxes and the line through them the model of the synchrotron radiation. The "bow tie" is the Chandra measured boundary of the X-ray spectrum (these error lines are 90% confidence after freezing N_H at its best fit value, which coincides with the Galactic column). The solid line is the predicted SSC spectrum for $\gamma_{min} = 1$ and the dashed line for $\gamma_{min} = 100$.

Fig. 8.— A color representation of the softness ratio (i.e., 1–2 keV/2–8 keV) in the region covered by the S3 chip superposed on X-ray contours of the background-subtracted image in the 0.75–8 keV band. The X-ray image has been adaptively smoothed with a 2-d Gaussian profile of varying width. The vertical bar indicates the relation between color and softness ratio, and the pixels were rebinned so that the fractional error in the ratio did not exceed 0.1. The contours indicate $2.5^n \times 10^{-2}$ cts pixel^{-1}, where $n = 1, 2, 3, 4, 5, 6, 7$, and 8.

Fig. 9.— The deprojected properties of the intracluster gas in individual shells surrounding the radio galaxy. For each ellipsoidal shell, the radius is the average of the semi-major and semi-minor axis. Top: Gas temperature (crosses) and electron density (solid line). Bottom: Metal Abundance (crosses) and thermal gas pressure (solid line).

Fig. 10.— The integrated mass profiles M($< $ r) of the cluster (solid and dashed lines), assuming

hydrostatic equilibrium and spherical symmetry, and the intracluster gas (dotted line) for radii between 80 and 500 kpc. The solid and dashed lines are for different assumed temperature profiles (see Paper III).

Fig. 11.— An unsmoothed image of the central region of the Cygnus A field in the 0.75–8 keV band. The shade is proportional to the square root of the intensity. The shading ranges from 0 (white) cts pixel^{-1} to 15 (black) cts pixel^{-1}. The areas indicated by solid lines mark regions from which spectra of the X-ray emission were extracted and modelled with mekals; the numbers indicate the resulting gas temperature in keV. Temperatures and regions marked in blue are hotter than the temperature of the innermost cluster shell (4.9 keV), while those marked in red are cooler. It is notable that the hotter regions are associated with the limb-brightened edges of the cavity, while the cooler regions are in the "belts" which encircle the cavity approximately along its minor axis.

Fig. 12.— Top: A simulation of the observed X-ray emission in the 0.75 - 8 keV band from the model of the cluster. The cavity was assumed to radiate no X-ray emission. Bottom: The difference between the observed image and the model given above. Some of the black regions are negative and result from the idealised modelling (as an ellipse) of the shape of the cavity. The color scale is in cts s^{-1} pixel^{-1}.
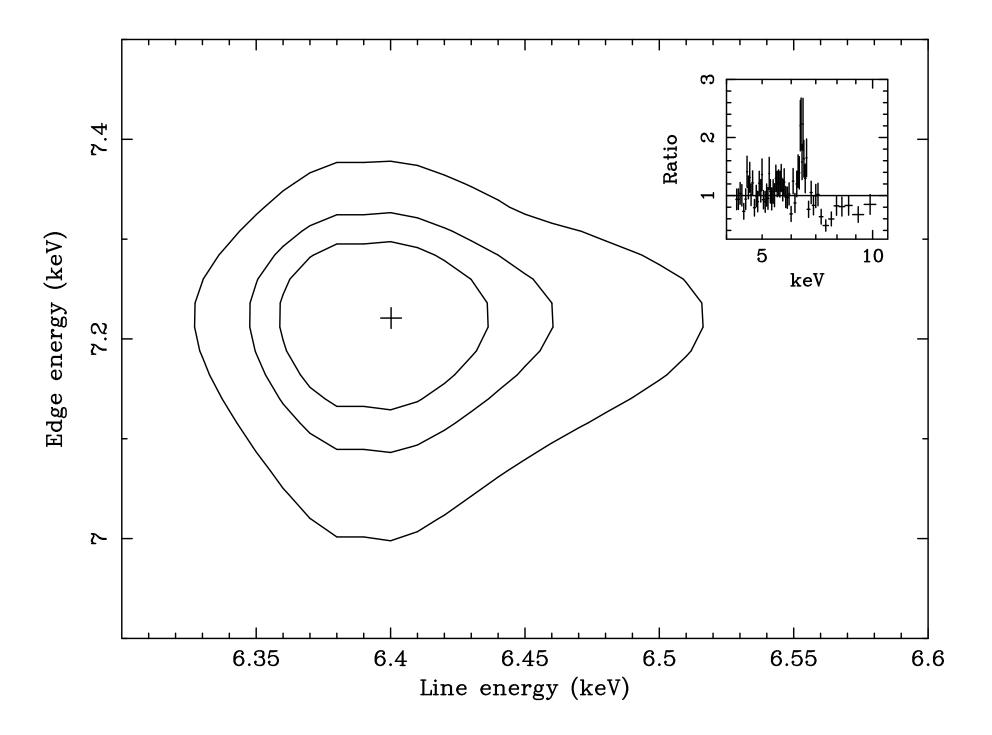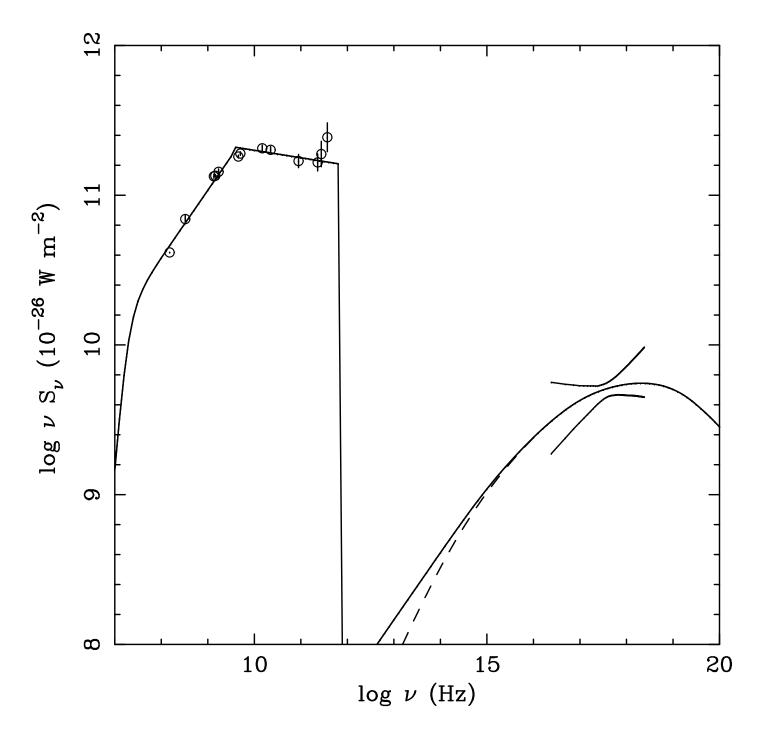
This figure "awilson-C2_fig1.jpg" is available in "jpg" format from:

http://arXiv.org/ps/astro-ph/0202319
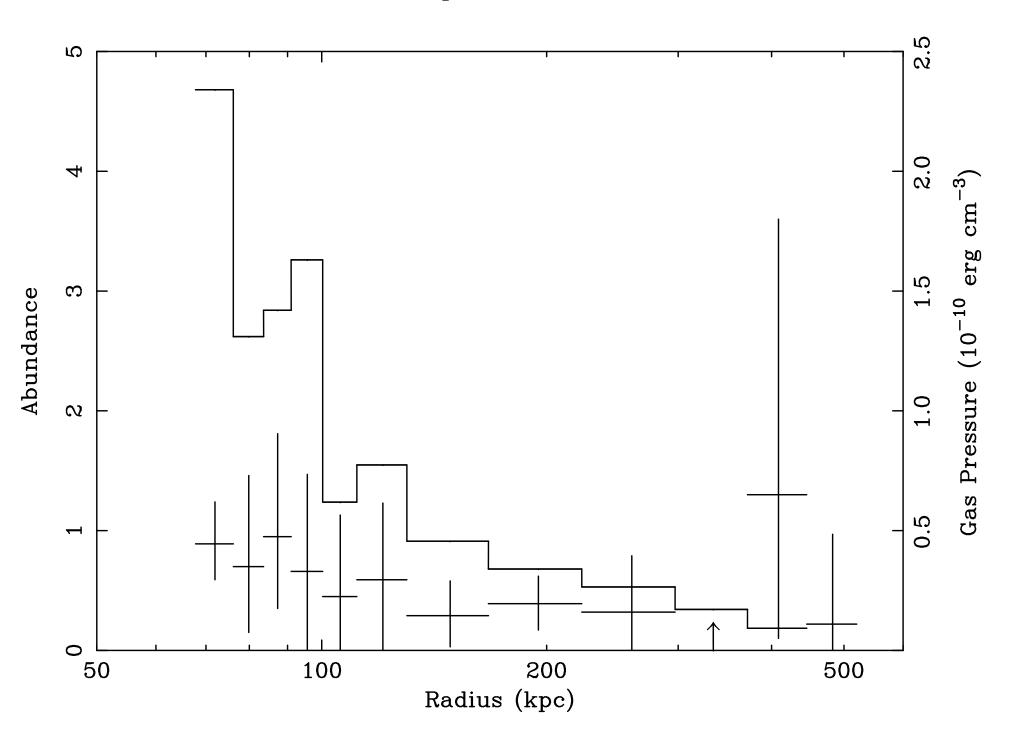
This figure "awilson-C2_fig2.jpg" is available in "jpg" format from:

http://arXiv.org/ps/astro-ph/0202319

This figure "awilson-C2_fig3.jpg" is available in "jpg" format from:

http://arXiv.org/ps/astro-ph/0202319

This figure "awilson-C2_fig4.jpg" is available in "jpg" format from:

http://arXiv.org/ps/astro-ph/0202319

This figure "awilson-C2_fig6.jpg" is available in "jpg" format from:

http://arXiv.org/ps/astro-ph/0202319

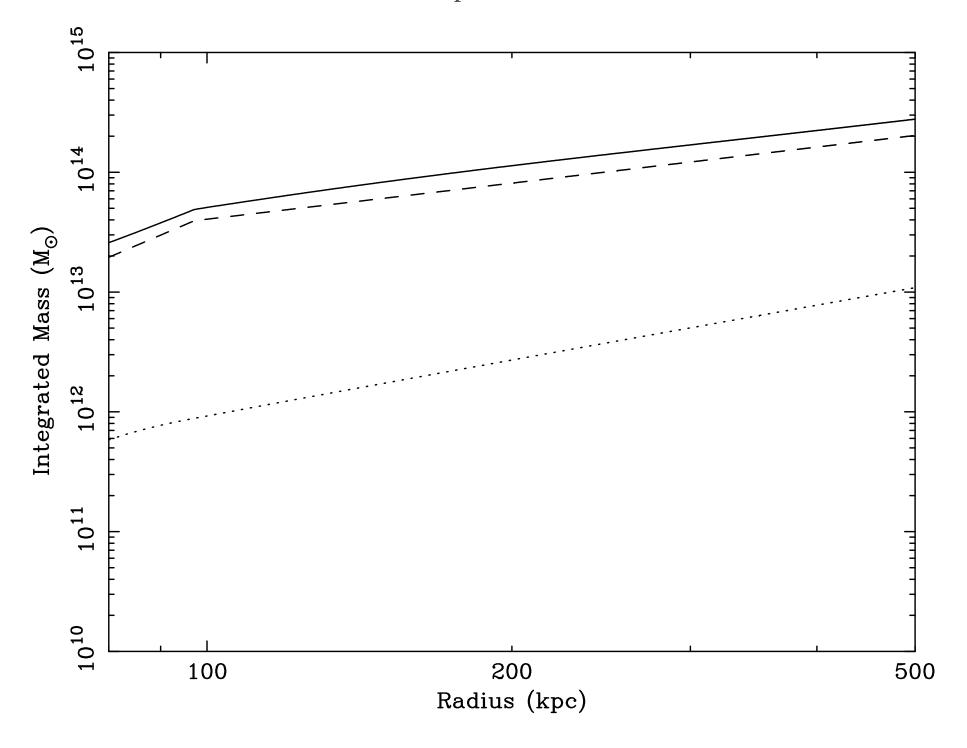This figure "awilson-C2_fig8.jpg" is available in "jpg" format from:

http://arXiv.org/ps/astro-ph/0202319

This figure "awilson-C2_fig11.jpg" is available in "jpg" format from:

http://arXiv.org/ps/astro-ph/0202319

This figure "awilson-C2_fig12bottom.jpg" is available in "jpg" format from:

http://arXiv.org/ps/astro-ph/0202319

This figure "awilson-C2_fig12top.jpg" is available in "jpg" format from:

http://arXiv.org/ps/astro-ph/0202319